

Theory of magnetic response in finite two-dimensional superconductors

F. Sebastián Bergeret^{1,2} and Ilya V. Tokatly^{3,4,2}

¹*Centro de Física de Materiales (CFM-MPC), Centro Mixto CSIC-UPV/EHU, Manuel de Lardizabal 4, E-20018 San Sebastián, Spain*

²*Donostia International Physics Center (DIPC), Manuel de Lardizabal 5, E-20018 San Sebastián, Spain*

³*Nano-Bio Spectroscopy group, Dpto. Física de Materiales, Universidad del País Vasco, Av. Tolosa 72, E-20018 San Sebastián, Spain*

⁴*IKERBASQUE, Basque Foundation for Science, E-48011 Bilbao, Spain*

We present a theory of magnetic response in a finite-size two-dimensional superconductors with Rashba spin-orbit coupling. The interplay between the latter and an in-plane Zeeman field leads on the one hand to an out-of-plane spin polarization which accumulates at the edges of the sample over the superconducting coherence length, and on the other hand, to circulating supercurrents decaying away from the edge over a macroscopic scale. In a long finite stripe of width W both, the spin polarization and the currents, contribute to the total magnetic moment induced at the stripe ends. These two contributions scale with W and W^2 respectively, such that for sufficiently large samples it can be detected by current magnetometry techniques.

Superconductivity in two-dimensional (2D) and quasi-2D systems has been attracting a great deal of attention over past decades [1, 2]. Examples of such systems range from ultra-thin metallic films, heavy fermion superlattices, and interfacial superconductors to atomic layers of metal dichalcogenides, and organic conductors.

Most 2D superconductors exhibit large spin-orbit coupling (SOC) because of broken space inversion symmetry. In this regard two types of 2D superconductors can be distinguished: Those exhibiting SOC of Rashba-type due to a broken up-down (out-of-plane) mirror symmetry, denoted here as Rashba superconductors, and those, in which a 2D in-plane inversion symmetry is broken due to a non-centrosymmetric crystal structure. The latter are exemplified by 2D transition metal dichalcogenides [3, 4]. To the first group, on which we focus here, belong for example ultra-thin superconducting metallic films [5–7].

Over the last years Rashba superconductors have been intensively studied as paradigmatic systems where pair correlations coexist with strong intrinsic SOC [8–20]. Because of the interplay between SOC and a Zeeman field they demonstrate highly unusual properties, such as, the appearance of an inhomogeneous superconducting phase [15, 17], magnetoelectric effects [9, 11, 20], and anisotropic magnetic susceptibility [12]. With few exceptions, as for example Refs. [18, 19, 21], most of these works focused on infinite 2D systems.

In this letter we demonstrate that finite size effects drastically modify the magnetic response of Rashba superconductors leading to hitherto unknown phenomena. Our main findings are the following: (i) In a response to a Zeeman field the system exhibits a spin texture (Fig. 1a) with a transverse component of the spin localized near the edge on the scale of superconducting coherence length. (ii) Because of the spin-charge coupling mediated by the SOC, a non-homogenous charge current appears

in the system with a spatial distribution that depends on the direction of the applied field and geometry of the system (Fig. 1b); (iii) In particular, for a finite stripe oriented along the field, macroscopic currents loops appear at the stripe ends (Fig. 1c). Both, the transverse spin and the edge currents contribute to the total magnetic moment which can be detected by state-of-the-art magnetometry techniques.

These findings can be qualitatively understood recalling the concepts of spin currents and spin galvanic effect (see Fig. 1). The key feature of 2D materials without up-down mirror symmetry is the Rashba SOC, $H_R = \alpha(\mathbf{e}_z \times \mathbf{v}) \cdot \boldsymbol{\sigma}$. Here \mathbf{e}_z is a vector normal to the 2D plane, $\mathbf{v} = \mathbf{p}/2m$ is the quasiparticle velocity, m its effective mass, $\boldsymbol{\sigma}$ is the vector of Pauli matrices, and α is the SOC constant [22]. The SOC acts as an effective \mathbf{p} -dependent spin splitting field. Let us assume that the system is subject to an external Zeeman field \mathbf{B} , and for some reason the induced spin polarization \mathbf{S} differs from the equilibrium Pauli response $\chi_P \mathbf{B}$, where χ_P is the Pauli paramagnetic polarizability. Then the excess spin $\delta \mathbf{S} = \mathbf{S} - \chi_P \mathbf{B}$ will experience an inhomogeneous precession in the effective Rashba field, generating a momentum anisotropy of the density matrix. In the presence of disorder the precession rate $\hat{R} = i[H_R, \delta \mathbf{S} \cdot \boldsymbol{\sigma}]$ is balanced by the momentum relaxation, which results in a steady spin current in the bulk of the system $\mathcal{J}_{bulk,k}^a = -\tau \text{tr} \langle v_k \sigma^a \hat{R} \rangle = \alpha D (\delta S^z \delta_{ka} - \delta S^k \delta_{az})$, where τ is the momentum relaxation time, and $D = \tau v_F^2 / 2$ is the diffusion coefficient. Under equilibrium conditions $\delta \mathbf{S} = 0$ in normal systems, but in superconductors pair correlations modify the Pauli response leading to a finite $\delta \mathbf{S}$ [12, 23]. This leads to finite equilibrium spin-currents in Rashba superconductors generated by the Zeeman field. For example, a field applied in x -direction in a bulk superconductor produces a spin-current with an out-of-plane polarization, $\mathcal{J}_{bulk,x}^z = -\alpha D \delta S^x$. Due to the spin-Hall

magneto-electric coupling in Rashba materials the bulk spin-current generates a transverse charge current according to $j_{bulk,y} \propto \alpha^2 \mathcal{J}_{bulk,x}^z = \alpha^3 D\delta S^x$, which is nothing, but the anomalous supercurrent well known for bulk superconductors with SOC [8, 11, 17].

In a finite system currents must vanish at the edges of the sample. This condition can be fulfilled only if the distribution of the excess spin $\delta\mathbf{S}(\mathbf{r})$ is inhomogeneous near the edge, so that the diffusion spin-current $\mathcal{J}_{diff,k}^a = -D\partial_k\delta S^a$ compensates the bulk contribution. For concreteness, if we assume a boundary with vacuum at $x = 0$, the zero spin-current condition for a field applied in x -direction reads: $D\partial_x\delta S^z = \mathcal{J}_{bulk,x}^z$, which implies that a finite component $\delta S^z(x)$ transverse to the field is induced at the edges of the sample. In this case the spin density exhibits a texture as sketched in Fig. 1a [24]. In the presence of SOC both the edge and the bulk spin-currents are converted into a charge current flowing parallel to the boundary, via the spin-galvanic effect, Fig. 1b. In a realistic finite system currents must vanish at all edges. The anomalous charge currents at the boundaries should then be compensated by supercurrents which stem from a gradient of the superconducting phase. As a consequence, in a stripe geometry, an in-plane field induces current loops at the edges as shown in Fig. 1c. The magnetic moment induced by this currents and by the transverse spin can in principle be measured to directly detect the effects we predict here. In the rest of the paper we provide a quantitative derivation of these effects, calculate the induced magnetic moment, and propose materials in which our predictions can be verified.

Specifically, we consider a 2D disordered superconductor with Rashba SOC. We assume that the Fermi energy corresponds to the largest energy scale, so that spectral and transport properties can be accurately described by the quasiclassical Green's functions (GFs) [25, 26]. In the diffusive limit these functions are isotropic in momentum and they obey the Usadel equation which in the presence of a Zeeman field and Rashba SOC reads [27–29]:

$$D\tilde{\nabla}_k \left(\tilde{g}\tilde{\nabla}_k\tilde{g} \right) - [(\omega + i\mathbf{h} \cdot \boldsymbol{\sigma})\tau_3 + \Delta\tau_2, \tilde{g}] = 0 \quad . \quad (1)$$

Here $\mathbf{h} = \mu_B\mathbf{B}$, $\boldsymbol{\sigma} = (\sigma^x, \sigma^y, \sigma^z)$ and $\tau_{2,3}$ are Pauli matrices spanning spin and Nambu space, respectively, ω is the Matsubara frequency, Δ is the superconducting order parameter, and SOC enters via the covariant derivative $\tilde{\nabla}_k\tilde{g} = \partial_k\tilde{g} - i[\hat{\mathcal{A}}_k, \tilde{g}]$, where $\hat{\mathcal{A}}_k = \alpha(\delta_{kx}\sigma^y - \delta_{ky}\sigma^x)$, summation over repeated indices is implied, and $k = x, y$ [30]. The quasiclassical GF \tilde{g} in Eq. (1) is a 4×4 matrix in the Nambu-spin space, which satisfies the normalization condition $\tilde{g}^2 = 1$. In the absence of spin-dependent fields it reads $\tilde{g}_0 = (\omega/E)\tau_3 + (\Delta/E)\tau_2$, where $E = \sqrt{\omega^2 + \Delta^2}$. It is easy to check by substitution into Eq. (1), that in the absence of Zeeman field \tilde{g}_0 is also the solution of the Usadel equation for arbitrary $\hat{\mathcal{A}}_k$.

To compute the response to an external magnetic field

we linearize Eq. (1) with respect to \mathbf{h} and write the solution as $\tilde{g} \approx \tilde{g}_0 + \delta\tilde{g}$. It is convenient to define $\delta\tilde{g} \equiv i\tilde{g}_0[\tau_3, \hat{Q}]$, where \hat{Q} is a matrix in spin space that satisfies the following equation [31]:

$$D\tilde{\nabla}_k^2\hat{Q} - 2E\hat{Q} = \mathbf{h} \cdot \boldsymbol{\sigma} \quad , \quad (2)$$

The excess spin density δS^a is then determined by [32]:

$$\delta S^a = -2\pi TN_F \sum_{\omega} \text{Tr}_{\sigma} \frac{\Delta^2}{E^2} \left[\sigma^a \hat{Q} \right] \quad . \quad (3)$$

For a homogeneous infinite 2D superconductor, the solution $\hat{Q}_b = Q_b^a \sigma^a$ of Eq. (2) reads

$$Q_b^z = -h^z [2E + 8D\alpha^2]^{-1} \quad (4)$$

$$Q_b^{x,y} = -h^{x,y} [2E + 4D\alpha^2]^{-1} \quad . \quad (5)$$

Equations (3)-(5) reproduce the bulk spin response of Rashba superconductor [12, 14], which is finite even at $T = 0$ and depends on the direction of the applied field.

This situation changes drastically in a finite system. First, we assume that the system is infinite in y -direction, and bounded to the region $|x| < L/2$ in the x -direction. The solution to Eq. (2) can be written as the sum of the bulk contribution and a contribution from the sample edges, $\hat{Q} = \hat{Q}_b + \delta\hat{Q}(x)$. According to Eq. (2) the latter satisfies:

$$D\partial_{xx}^2\delta Q^x - (4D\alpha^2 + 2E)\delta Q^x + 4D\alpha\partial_x\delta Q^z = 0 \quad (6)$$

$$D\partial_{xx}^2\delta Q^z - (8D\alpha^2 + 2E)\delta Q^z - 4D\alpha\partial_x\delta Q^x = 0 \quad . \quad (7)$$

The last terms in these equations describe precession of the excess spin, caused by SOC. Importantly, the precession terms are finite only for inhomogeneous systems. The boundary conditions to the above equations are obtained by imposing zero-current at the edges, $x = \pm L/2$ [28, 33]:

$$\partial_x\delta\hat{Q} - i\alpha \left[\sigma^y, \delta\hat{Q} \right] \Big|_{x=\pm L/2} = i\alpha \left[\sigma^y, \hat{Q}_b \right] \quad . \quad (8)$$

Here the left hand side is proportional to the inhomogeneous spectral spin-current which cancels the bulk one in the right hand side. The boundary problem of Eqs. (7)-(8) has a nontrivial solution only if the right-hand-side in Eq. (8), that is the bulk spin-current, is finite. According to Eqs. (4)-(5), this is the case when the magnetic field has either z - or x -components. How to obtain the solution for δQ^a is discussed in the Supplementary Material. Here we present the spatial dependence of the induced spin obtained from Eq. (3) and plotted in Figs. 2(a,c). Both for in-plane ($\mathbf{B} \parallel \mathbf{e}_x$), and for out-of-plane ($\mathbf{B} \parallel \mathbf{e}_z$) fields, in addition to the longitudinal spin, a transverse component of the spin-density is generated. The latter is localized at the edges of the sample with opposite sign on opposite sides and decay into the bulk over the coherence length ξ_s . These results generalize the theory of

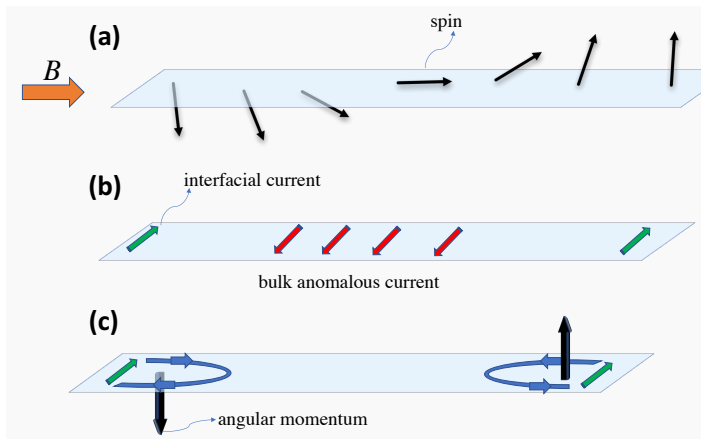


Figure 1. Schematically description of the magnetic response in finite size superconductors in the presence of an in-plane field B . (a) Black arrows represents the deviation of the spin density, δS , from the Pauli spin. Because of the SOC and the finite size of the sample a transverse component of δS is generated. (b) The spin-charge coupling due to the SOC induces bulk (red arrows) and edge (green arrows) charge supercurrents. (c) Due to the finite size of the sample the edge currents flow in close loops (blue), inducing an out-of-plane angular momentum (black arrows).

magnetic response for Rashba superconductors [12, 14] to the case of finite samples.

In addition to the finite spin response at $T = 0$, the SOC in superconductors also leads to the spin-galvanic effect, that is, a creation of charge currents by a Zeeman field [11, 17, 20, 34]. In the stripe geometry (see middle panels of Fig. 2) the so called anomalous charge current is induced in y -direction, $j_y^{an} = (\theta/m)(\partial_x \delta S^z - 2\alpha \delta S^x)$ [33], where $\theta = 2D\tau\alpha^2$ is a dimensionless parameter which in normal systems describes the spin-charge conversion [35]. Within the diffusive approximation it is a small parameter which we treat perturbatively. Here δS^a is obtained by substituting the solution of Eqs. (6)-(7) into Eq. (3). This results in

$$j_y^{an} = -4\pi\theta \frac{TN_F}{m} \sum_{\omega} \frac{\Delta^2}{E^2} (\partial_x \delta Q^z - 2\alpha \delta Q^x - 2\alpha Q_b^x) \equiv j_{edge}^{an}(x) + j_b^{an}. \quad (9)$$

In the second line we identify two contributions to the anomalous current: the bulk contribution j_b^{an} , widely studied in homogeneous superconductors [9, 11, 17, 20] and given by the last term in the brackets in the first line and (red arrows in middle panels in Fig. 2), and the boundary contribution j_{edge}^{an} , determined by the first two terms. The latter are localized at the edges of the sample within the scale of superconducting coherence length (green arrows in middle panels of Fig. 2). In the geometry under consideration, the "bulk" contribution to the current is finite only for fields applied across the stripe (x -direction).

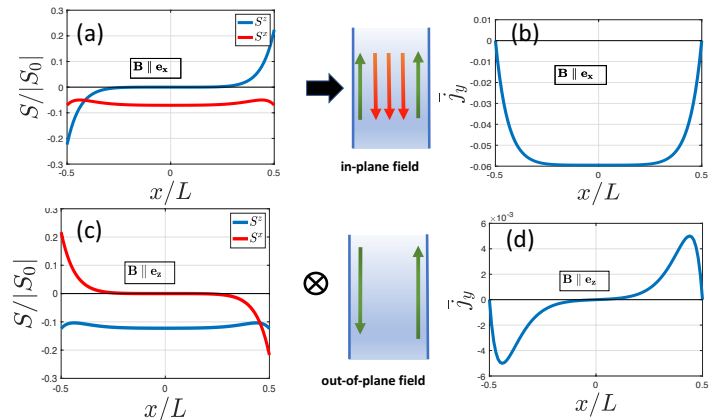


Figure 2. Spin density (panels a,c), and charge current density (panels b,d), induced by an in-plane (a-b) and out-of plane field (c-d), for $\alpha = 0.2\xi_0$, $L = 10\xi_0$. The middle panels shows schematically the corresponding bulk (red arrows) and edge currents (green arrows)

The spatial dependence of the charge current density is shown on Fig. 2 b and d for fields in x - and z -direction, respectively. Because of zero spin-current condition, Eq. (8), the charge current of Eq. (9) also vanishes at the boundaries. When the field is applied in x -direction, Fig. 2b, both, the bulk and edge contributions, are finite. The maximal value of the total current is the "bulk" value reached deeply inside the sample, away from the edges. The spatial distribution of the current is symmetric and the net current through the stripe is non-zero. In contrast, if the field is applied in z -direction, Fig. 2d, there is no bulk contribution, because Q_b^z does not contribute to the current, see Eq. (9). Only edge currents, opposite on opposite sides, appear. Clearly in this case the total charge current vanishes.

The above results apply for an infinite superconducting stripe, and whether the obtained currents may exist in real finite systems depends on transverse boundary conditions. For example, if the finite stripe is wrapped in a cylinder, the periodic boundary conditions indeed allow for the above current patterns when the field is applied along the the cylinder axis [17]. Here we consider a more experimentally relevant situation: a finite 2D superconductor of rectangular shape, which occupies the region $|x| < L/2$ and $|y| < W/2$ (see Fig. 3). Obviously, the charge current through all boundaries must vanish. For out-of-plane field this condition is trivially satisfied by closing the boundary streamlines, which generates a circulating edge current. However, in this situation, orbital effects also create circulating diamagnetic supercurrents and the detection of a pure anomalous current is rather difficult. Therefore, here we focus on the case of in-plane field. As shown in Fig. 2(b), in this case the anomalous current has the same direction at both edges. Hence, in the presence of impenetrable boundaries at $y = \pm W/2$,

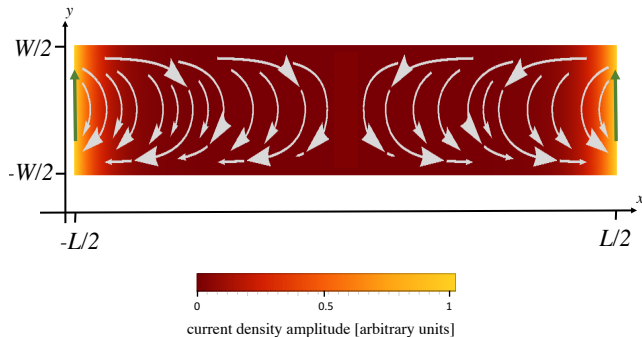


Figure 3. The current flow in a finite 2D superconductor with SOC when the field is applied in x -direction. The green arrows represents the edge contributions to the anomalous SH-current. The color-scale shows the decay of the current amplitude away from the interface.

one naturally expects generation of closed streamlines at each edge as shown schematically in Fig. 1(c). In what follows we study this situation quantitatively.

To satisfy the zero-current condition at $y = \pm W/2$, the anomalous current of Eq. (9) needs to be compensated by a supercurrent generated by a gradient of the superconducting phase $\varphi(\mathbf{r})$. The total charge current in a superconductor reads,

$$\mathbf{j}_k = \frac{n_s}{2m} \partial_k \varphi + \mathbf{j}_k^{an}, \quad (10)$$

where n_s is the superfluid density. Since the anomalous current is divergenceless, the continuity equation for the current reduces to the Laplace equation for the phase,

$$\nabla^2 \varphi = 0 \quad (11)$$

which has to be solved by imposing a zero current condition at the edges of the sample,

$$n_k \partial_k \varphi|_{edge} = - \frac{2m}{n_s} n_k j_k^{an} \Big|_{edge} \quad (12)$$

where \mathbf{n} is a unit vector normal to the edge. The boundary problem, Eqs. (11)-(12), can be solved following the procedure described in Refs. [35, 36]. Here we present the results for a narrow stripe oriented along x -axis with $\xi_s \ll L \ll W$. In this case the currents near opposite edges at $x = \pm L/2$ are independent from each-other, and one can treat each edge separately. For the current near the left edge at $x = -L/2$ we find,

$$j_y(x, y) = I_y^{edge} \int \frac{dk}{2\pi} e^{ik(x+L/2)} \left[1 - \frac{\cosh ky}{\cosh kW/2} \right] \quad (13)$$

$$j_x(x, y) = -i I_y^{edge} \int \frac{dk}{2\pi} e^{ik(x+L/2)} \frac{\sinh ky}{\cosh kW/2}, \quad (14)$$

where I_y^{edge} is the net anomalous edge current, obtained by integrating $j_{edge}^{an}(x)$ in Eq. (9) from the boundary

($x = -L/2$) to the bulk of the sample ($x = 0$). Fig. 3 shows the current streamlines in the whole stripe obtained from these equations. One identifies two different scales: (i) a mesoscopic scale of the order of the coherence length ξ_s , over which the anomalous current $j_{edge}^{an}(x)$ decays, and (ii) a macroscopic scale related to the size of the sample. In the present limiting case, $\xi_s \ll L \ll W$, there are two clearly defined contributions to the y -component of the current: the edge anomalous current localized at the boundary (first term in the integrand of Eq. (13) represented by a green arrow in Fig. 3), and the counterflow of supercurrent given by the second term in Eq. (13), which decays over the scale $\sim W$ and compensates the anomalous edge component such that $\int dx j_y(x, y) = 0$.

The current stream generates a finite orbital angular momentum \mathcal{L}_z , see Fig. 1c. The latter is computed from its general definition $\mathcal{L}_z = m \int \int dx dy (x j_y - y j_x)/2$, and scales as W^2 :

$$\mathcal{L}_z = -m \frac{W^2}{4} I_y^{edge} \int \frac{dk \tanh^2 k}{2\pi k^2} \approx -m \frac{W^2}{8} I_y^{edge}. \quad (15)$$

Similarly the total spin angular momentum accumulated at the edge is obtained by integrating the z -component of the spin, Eq. (3), $\mathcal{S}_z = \int_{-L/2}^0 \delta S^z(x) dx$.

In the Supplementary Material we derive the following analytical expressions for both the spin and orbital angular momenta at $T = 0$ in two limiting cases:

$$\mathcal{S}_z \propto -N_F h_x W \xi_0 \begin{cases} \xi_0 \alpha, & \text{for } \xi_0 \alpha \ll 1 \\ (\alpha \xi_0)^{-3}, & \text{for } \xi_0 \alpha \gg 1, \end{cases} \quad (16)$$

and

$$\mathcal{L}_z \propto -N_F h_x \theta W^2 \begin{cases} \xi_0 \alpha, & \text{for } \xi_0 \alpha \ll 1 \\ (\xi_0 \alpha)^{-4} \ln(\xi_0 \alpha), & \text{for } \xi_0 \alpha \gg 1 \end{cases} \quad (17)$$

with $\xi_0 = \sqrt{D/2\Delta}$. The measurable magnetic moment is then given by $\mathcal{M}_z = \mu_B (\mathcal{L}_z/\hbar + \mathcal{S}_z)$, where μ_B is the Bohr magneton [37]. Both contributions have the same sign. However, the spin angular momentum scales with W , while \mathcal{L}_z scales with W^2 and therefore dominates in macroscopic samples.

In conclusion, we presented a complete theory of the magnetic response of finite size Rashba superconductors. When the field is applied in-plane our theory predicts on the one hand a finite out-of-plane spin polarization localized at the edge of the sample on the scale of superconducting coherence length. On the other hand, the SOC also leads to supercurrents circulating in the sample. Both the spin and the orbital momentum of supercurrents contribute to the total magnetic moment, which is induced at the edges and can be measured by state-of-the-art magnetic sensors [38, 39]. Whereas the contribution from the spin angular momentum scales with the width W of a rectangular stripe, the contribution from the currents scales with W^2 and therefore dominates in

large samples. There are several superconducting materials with Rashba SOC and which our findings can be verified. These range from Pb and Tl-Pb monolayers [6, 40–42], to thin MoS₂, NbRe, β -Bi₂Pd films [43–45], and 2D superconductivity at the LaAlO₃/SrTiO₃ interface [46–49].

Acknowledgements.— We acknowledge funding by the Spanish Ministerio de Ciencia, Innovación y Universidades (MICINN) (Projects No. FIS2016-79464-P and No. FIS2017-82804-P), by Grupos Consolidados UPV/EHU del Gobierno Vasco (Grant No. IT1249-19), and by EU’s Horizon 2020 research and innovation program under Grant Agreement No. 800923 (SUPERTEED).

-
- [1] T. Uchihashi, Superconductor Science and Technology **30**, 013002 (2016).
- [2] Y. Saito, T. Nojima, and Y. Iwasa, Nature Reviews Materials **2**, 16094 (2017).
- [3] Y. Saito, Y. Nakamura, M. S. Bahramy, Y. Kohama, J. Ye, Y. Kasahara, Y. Nakagawa, M. Onga, M. Tokunaga, T. Nojima, *et al.*, Nature Physics **12**, 144 (2016).
- [4] J. Lu, O. Zheliuk, I. Leermakers, N. F. Yuan, U. Zeitler, K. T. Law, and J. Ye, Science **350**, 1353 (2015).
- [5] D. V. Gruznev, L. V. Bondarenko, A. V. Matetskiy, A. A. Yakovlev, A. Y. Tupchaya, S. V. Ereemeev, E. V. Chulkov, J.-P. Chou, C.-M. Wei, M.-Y. Lai, *et al.*, Scientific reports **4**, 4742 (2014).
- [6] T. Sekihara, R. Masutomi, and T. Okamoto, Physical review letters **111**, 057005 (2013).
- [7] G. C. Ménard, S. Guissart, C. Brun, R. T. Leriche, M. Trif, F. Debontridder, D. Demaille, D. Roditchev, P. Simon, and T. Cren, Nature communications **8**, 2040 (2017).
- [8] V. Edelstein, Soviet Physics-JETP (English Translation) **68**, 1244 (1989).
- [9] V. M. Edelstein, Physical review letters **75**, 2004 (1995).
- [10] V. M. Edelstein, Journal of Physics: Condensed Matter **8**, 339 (1996).
- [11] S. Yip, Physical Review B **65**, 144508 (2002).
- [12] L. P. Gor’kov and E. I. Rashba, Phys. Rev. Lett. **87**, 037004 (2001).
- [13] P. Frigeri, D. Agterberg, and M. Sigrist, New Journal of Physics **6**, 115 (2004).
- [14] V. M. Edelstein, Physical Review B **78**, 094514 (2008).
- [15] D. Agterberg and R. Kaur, Physical Review B **75**, 064511 (2007).
- [16] O. V. Dimitrova and M. V. Feigelman, Journal of Experimental and Theoretical Physics Letters **78**, 637 (2003).
- [17] O. Dimitrova and M. Feigel’Man, Physical Review B **76**, 014522 (2007).
- [18] S. S. Pershoguba, K. Björnson, A. M. Black-Schaffer, and A. V. Balatsky, Phys. Rev. Lett. **115**, 116602 (2015).
- [19] A. G. Mal’shukov, Phys. Rev. B **93**, 054511 (2016).
- [20] F. Konschelle, I. V. Tokatly, and F. S. Bergeret, Phys. Rev. B **92**, 125443 (2015), arXiv:1506.02977.
- [21] V. M. Edelstein, Physical Review B **67**, 020505 (2003).
- [22] In our notation α has dimensions of momentum and it is proportional to the usual Rashba constant $\alpha_R = \alpha/m$. Throughout the article we choose the z -axis as the axis perpendicular to the superconductor plane.
- [23] A. A. Abrikosov and L. P. Gor’kov, Sov. Phys. JETP. **15**, 752 (1962).
- [24] I. V. Tokatly, B. Bujnowski, and F. Bergeret, arXiv preprint arXiv:1901.07890 (2019).
- [25] G. Eilenberger, Zeitschrift für Physik **214**, 195 (1968).
- [26] A. Larkin and Y. N. Ovchinnikov, Sov Phys JETP **28**, 1200 (1969).
- [27] F. S. Bergeret, A. F. Volkov, and K. B. Efetov, **77**, 1321 (2005), arXiv:0506047 [cond-mat].
- [28] F. S. Bergeret and I. V. Tokatly, Physical Review Letters **110**, 1 (2013), arXiv:1211.3084.
- [29] F. S. Bergeret and I. V. Tokatly, Physical Review B **89**, 134517 (2014), arXiv:1402.1025.
- [30] If the magnetic field has a component out-of-plane one should include in Eq. (1) the usual U(1) vector potential which leads to orbital effects. Here we are interesting in the spin-magnetic response and neglect orbital terms.
- [31] In deriving Eq. (2) we used the linearized normalization condition $\tilde{g}_0\delta\tilde{g} + \delta\tilde{g}\tilde{g}_0 = 0$.
- [32] The deviation from the Pauli response, $\delta\mathbf{S} = \mathbf{S} - \chi_P\mathbf{B}$, is determined by $\delta S^a = -(i/2)\pi TN_F \sum_{\omega} \text{Tr}[\tau_3\sigma^a\delta g]$, where $\chi_P = -2N_F\mu_B$, and N_F is the density of states at the Fermi level. In the normal state $\delta\mathbf{S} = 0$ and therefore the generated magnetic moment is $M_0 = -\mu_B\chi_P B$. In the superconducting state at zero temperature and zero SOC $\delta S = -\chi_P B$ and hence the total magnetization is zero.
- [33] I. V. Tokatly, Physical Review B **96**, 060502 (2017).
- [34] V. M. Edelstein, Physical Review B **72**, 172501 (2005).
- [35] C. Sanz-Fernández, J. Borge, I. V. Tokatly, and F. S. Bergeret, arXiv preprint arXiv:1907.11688 (2019).
- [36] J. Borge and I. V. Tokatly, Physical Review B **99**, 241401 (2019).
- [37] The spin magnetic moment is given by $\mu_{\text{spin}} = (-g|e|/2m)(\hbar/2)\sigma = \mu_B\sigma$.
- [38] C. Granata and A. Vettoliere, Physics Reports **614**, 1 (2016).
- [39] P. Maletinsky, S. Hong, M. S. Grinolds, B. Hausmann, M. D. Lukin, R. L. Walsworth, M. Loncar, and A. Yacoby, Nature nanotechnology **7**, 320 (2012).
- [40] S. Qin, J. Kim, Q. Niu, and C.-K. Shih, Science **324**, 1314 (2009).
- [41] C. Brun, T. Cren, V. Cherkez, F. Debontridder, S. Pons, D. Fokin, M. Tringides, S. Bozhko, L. Ioffe, B. Altshuler, *et al.*, Nature Physics **10**, 444 (2014).
- [42] A. Matetskiy, S. Ichinokura, L. Bondarenko, A. Tupchaya, D. Gruznev, A. Zotov, A. Saranin, R. Hobara, A. Takayama, and S. Hasegawa, Physical review letters **115**, 147003 (2015).
- [43] N. F. Yuan, K. F. Mak, and K. Law, Physical review letters **113**, 097001 (2014).
- [44] C. Cirillo, G. Carapella, M. Salvato, R. Arpaia, M. Caputo, and C. Attanasio, Physical Review B **94**, 104512 (2016).
- [45] Y.-F. Lv, W.-L. Wang, Y.-M. Zhang, H. Ding, W. Li, L. Wang, K. He, C.-L. Song, X.-C. Ma, and Q.-K. Xue, Science bulletin **62**, 852 (2017).
- [46] D. Dikin, M. Mehta, C. Bark, C. Folkman, C. Eom, and V. Chandrasekhar, Physical Review Letters **107**, 056802 (2011).
- [47] J. A. Bert, B. Kalisky, C. Bell, M. Kim, Y. Hikita, H. Y.

- Hwang, and K. A. Moler, Nature physics **7**, 767 (2011).
 [48] B. Kalisky, J. A. Bert, B. B. Klopfer, C. Bell, H. K. Sato, M. Hosoda, Y. Hikita, H. Y. Hwang, and K. A. Moler, Nature communications **3**, 922 (2012).
 [49] S. Hurand, A. Jouan, C. Feuillet-Palma, G. Singh, J. Biscaras, E. Lesne, N. Reyren, A. Barthélemy, M. Bibes, J. Villegas, *et al.*, Scientific reports **5**, 12751 (2015).

Appendix A: Solution of the boundary problem Eqs. (6-8)

In the main text all observables, currents, angular momenta, etc, are expressed in terms of $\delta\mathbf{S}$, which is the deviation of the spin-density from the Pauli paramagnetic spin. According to Eq. (3), the components of $\delta\mathbf{S}$ are determined from the matrix \hat{Q} . there are two types of contributions: One stemming from the bulk of the sample, \hat{Q}_b and another one from the boundary, $\delta\hat{Q}$. The latter is obtained by solving the boundary problem Eqs. (6-8). Here we describes the main features of the solution procedure.

The precession term in Eqs. (6-7) couples the x and z components, $\delta Q^{x,z}$. These components are also coupled via the boundary condition, Eq. (8), which written explicitly reads:

$$\begin{aligned}\partial_x \delta Q^z - 2\alpha \partial \delta Q^x|_{x=\pm L/2} &= 2\alpha Q_b^x \\ \partial_x \delta Q^x + 2\alpha \partial \delta Q^z|_{x=\pm L/2} &= -2\alpha Q_b^z\end{aligned}\quad (S1)$$

Clearly, a nontrivial solution exists only if the right-hand-side in these equation is non-zero. This is the case when the magnetic field has either z - or x -components.

It is straightforward to check that the general solution for the boundary quantity, δQ^a , reads

$$\begin{aligned}\delta Q^a &= A_+^a e^{\kappa_+(x+L/2)} + B_+^a e^{-\kappa_+(x+L/2)} + A_-^a e^{\kappa_-(x+L/2)} + \\ &+ B_-^a e^{-\kappa_-(x+L/2)},\end{aligned}\quad (S2)$$

where $\kappa_\pm = \sqrt{\kappa_E^2 - 2\alpha^2 \pm 2i\alpha\sqrt{7\alpha^2 + 4\kappa_E^2}}$, $\kappa_E^2 = 2E/D$, and $\text{Re}\kappa_\pm > 0$, is the characteristic length over which δQ decays away from the edge. Then, the transverse spin induces at the edge of the sample decays into bulk over a distance that we denote ξ_s . At low temperatures:

$$\xi_s \approx \frac{1}{\text{Re}\sqrt{\frac{1}{\xi_0^2} - 2\alpha^2 + i\alpha\sqrt{7\alpha^2 + \frac{4}{\xi_0^2}}}},\quad (S3)$$

where $\xi_0 = \sqrt{D/2\Delta}$.

For sufficiently large L , the solution near each boundary can be found independently. For example the solution at the $x = -L/2$ boundary consists only on the decaying exponents with

$$\begin{aligned}\delta Q^z(x) &= B_+^z e^{-\kappa_+x} + B_-^z e^{-\kappa_-x} \\ \delta Q^x(x) &= B_+^x e^{-\kappa_+x} + B_-^x e^{-\kappa_-x},\end{aligned}\quad (S4)$$

with

$$B_\pm^x = \frac{4\alpha\kappa_\pm}{\kappa_\pm^2 - 4\alpha^2 - \kappa_E^2} B_\pm^z. \quad (S5)$$

The coefficients B_\pm^z are then determined by Eqs. (S1). The solution, Eq. (S4), describes the spin density accumulated at the edge of the sample, $x = -L/2$, and decays into the bulk over the superconducting coherence length, and eventually oscillates. In Fig. 2(a,c) of the main text we show the total spin-density obtained by substituting the solution Eq. (S4) into Eq. (3) of the main text.

Appendix B: Calculation of the angular momenta, Eqs. (15-17)

In this section we calculate the total angular momentum at the left edge, $x = -L/2$ of the stripe shown in Fig. 3 when $\xi_0 \ll W \ll L$. Because both, the anomalous current and spin densities generated at the boundary, decay into the bulk over the coherence length ξ_0 the integrals in Eqs. (16-17) of the main text is can be taken in the interval $-L/2 < x < 0$. We first determined the total orbital angular momentum \mathcal{L}_z given in Eq. (15) which is proportional to the contribution to the anomalous current stemming from the boundary of the sample, denoted in the main text as I_y^{edge} , and defined in Eq. (16). After substituting the expression j_{edge}^{an} from Eq. (9) we obtain:

$$I_y^{edge} = -4\pi\theta \frac{TN_F}{m} \sum_\omega \frac{\Delta^2}{E^2} [-\delta Q^z(-L/2) - 2\alpha\overline{\delta Q^x}], \quad (S6)$$

where $\overline{\delta Q^x} = \int_{-L/2}^0 dx \delta Q^x(x)$ and can be determined by integrating the Usadel equation, Eq. (6) in the same interval:

$$-\partial_x \delta Q^x(-L/2) - (4\alpha^2 + \kappa_E^2)\overline{\delta Q^x} - 4\alpha\delta Q^z(-L/2) = 0. \quad (S7)$$

According to the boundary condition Eq. (8), the first term of the latter equation equals

$$-\partial_x \delta Q^x(-L/2) = 2\alpha\delta Q^z(-L/2),$$

and therefore

$$\overline{\delta Q^x} = -\frac{2\alpha}{4\alpha^2 + \kappa_E^2} \delta Q^z(-L/2), \quad (S8)$$

After substitution into Eq. (S6) we can write the anomalous boundary current in terms of δQ^z at $x = -L/2$:

$$I_y^{edge} = 4\pi\theta \frac{TN_F}{m} \sum_\omega \frac{\Delta^2}{E^2} \frac{\kappa_E^2}{4\alpha^2 + \kappa_E^2} \delta Q^z(-L/2) \quad (S9)$$

Finally one obtains the total orbital angular momentum from Eq. (15):

$$\mathcal{L}_z = -\frac{\pi}{2}\theta W^2 TN_F \sum_\omega \frac{\Delta^2}{E^2} \frac{\kappa_E^2}{4\alpha^2 + \kappa_E^2} \delta Q^z(-L/2) \quad (S10)$$

Equivalently one can also express the total boundary spin, \mathcal{S}_z in terms of the boundary value $\delta Q^x(-L/2)$. For this sake we first integrate the Usadel equation (7) which together with the boundary condition (8) gives an expression for the integrated δQ^z :

$$\overline{\delta Q^z} = 2\alpha \frac{\delta Q^x(-L/2) - Q_b^x}{8\alpha^2 + \kappa_E^2}. \quad (\text{S11})$$

This expression together with Eq. (3) gives the total spin angular momentum

$$\mathcal{S}_z = -8\pi TN_F W \alpha \sum_{\omega} \frac{\Delta^2}{E^2} \frac{\delta Q^x(-L/2) - Q_b^x}{8\alpha^2 + \kappa_E^2} \quad (\text{S12})$$

Expressions (S10) and (S12) express the angular momenta in terms of the values of the the functions δQ^a , $a = x, z$, at the boundary of the sample. These can be obtained by solving the boundary problem Eqs. (6-8). In the case under consideration, $\xi_s \ll W \ll L$, only terms which decay away from the boundary in Eq. (S2) contribute to the solution:

$$\delta Q^a = B_+^a e^{-\kappa_+(x+L/2)} + B_-^a e^{-\kappa_-(x+L/2)}, \quad (\text{S13})$$

with $a = x, z$, and

$$B_{\pm}^x = \frac{4\alpha\kappa_{\pm}}{\kappa_{\pm}^2 - 4\alpha^2 - \kappa_E^2} B_{\pm}^z. \quad (\text{S14})$$

The coefficients B_{\pm}^z are obtained from the boundary condition, Eq. (8):

$$(B_-^z)^* = B_+^z = \frac{-i\alpha Q_b^x (\kappa_+^2 - 4\alpha^2 - \kappa_E^2) (\kappa_-^2 + 4\alpha^2 + \kappa_E^2)}{\text{Im} [\kappa_- (\kappa_+^2 + 4\alpha^2 + \kappa_E^2) (\kappa_-^2 + 4\alpha^2 - \kappa_E^2)]}, \quad (\text{S15})$$

and hence

$$\delta Q^z(-L/2) = 2\alpha Q_b^x \frac{\text{Im} [(\kappa_+^2 - 4\alpha^2 - \kappa_E^2) (\kappa_-^2 + 4\alpha^2 + \kappa_E^2)]}{\text{Im} [\kappa_- (\kappa_+^2 + 4\alpha^2 + \kappa_E^2) (\kappa_-^2 + 4\alpha^2 - \kappa_E^2)]} \quad (\text{S16})$$

and

$$\delta Q^x(-L/2) = 8\alpha^2 Q_b^x \frac{\text{Im} [\kappa_+ (\kappa_-^2 + 4\alpha^2 + \kappa_E^2)]}{\text{Im} [\kappa_- (\kappa_+^2 + 4\alpha^2 + \kappa_E^2) (\kappa_-^2 + 4\alpha^2 - \kappa_E^2)]} \quad (\text{S17})$$

By substituting Eqs. (S16) and (S17) into Eqs. (S10) and (S12) one can obtain, after summing over frequencies, the total orbital and spin angular momentum respectively. In order to obtain analytical expressions here consider two limiting cases:

Small SOC: $\alpha \ll \kappa_E$

In this case

$$\delta Q^z(-L/2) \approx -\frac{\alpha}{\kappa_E} Q_b^x, \quad (\text{S18})$$

and from Eq. (S10) we obtain:

$$\mathcal{L}_z \approx \pi W^2 TN_F D \tau \alpha^2 \sum_{\omega} \frac{\Delta^2}{E^2} \frac{\kappa_E^2}{\kappa_E^2} \frac{\alpha}{\kappa_E} Q_b^x. \quad (\text{S19})$$

At low temperature, $t \rightarrow 0$, the sum can be written as an integral over frequencies. After substitution of the bulk value Q_b^x , Eq. (5) in the main text, we obtain (compare with Eq. (19) in the main text):

$$\mathcal{L}_z \approx -h^x \alpha \xi_0 W^2 N_F \frac{\theta}{8} \int d\omega \frac{1}{(\omega^2 + 1)^{7/2}}, \quad (\text{S20})$$

where $\xi_0 = \sqrt{D/2\Delta}$ and the numerical factor is obtained by evaluation of the integral:

$$\frac{1}{8} \int d\omega \frac{1}{(\omega^2 + 1)^{7/2}} = \frac{1}{8} \frac{\sqrt{\pi} \Gamma(5/4)}{\Gamma(7/4)} \approx 0.21. \quad (\text{S21})$$

On the other hand the total spin \mathcal{S}_z is obtain from Eq. (S12). In leading order in $\alpha \xi_0$ only the Q_b^x contributes:

$$\mathcal{S}_z \approx -8\pi TN_F W \alpha h^x \sum_{\omega} \frac{\Delta^2}{E^2} \frac{1}{2E\kappa_E^2}, \quad (\text{S22})$$

which at low temperatures reduces to (*cf.* with Eq. (18) in the main text)

$$\mathcal{S}_z \approx -2N_F W \alpha h^x \xi_0^2 \int d\omega \frac{1}{(\omega^2 + 1)^2} \approx -\pi N_F W \alpha h^x \xi_0^2. \quad (\text{S23})$$

Large SOC: $\alpha \gg \kappa_E$

In this limiting case the total spin, \mathcal{S}_z can be calculated straightaway from Eq. (S12), by taking everywhere leading order terms in κ_E/α . Specifically, from Eq. (S17)

$$\delta Q^x(-L/2) \approx (\sqrt{2} - 1) Q_b^x, \quad (\text{S24})$$

whereas

$$\delta Q^z(-L/2) \approx -\sqrt{\sqrt{8} - 1} Q_b^x. \quad (\text{S25})$$

Substituting these expressions into Eqs. (S12,S10), and considering the low temperature regime we obtain:

$$\begin{aligned} \mathcal{S}_z &\approx \frac{N_F W}{\alpha} \left(1 - \frac{1}{\sqrt{2}}\right) \Delta^2 Q_b^x \int \frac{d\omega}{\omega^2 + \Delta^2} \\ &\approx \frac{N_F W}{\alpha} \left(1 - \frac{1}{\sqrt{2}}\right) \pi \Delta Q_b^x \end{aligned} \quad (\text{S26})$$

and within logarithmic accuracy:

$$\mathcal{L}_z \approx W^2 N_F \tau \Delta^2 \ln(\xi_0 \alpha) \sqrt{\sqrt{8} - 1} Q_b^x. \quad (\text{S27})$$

According to Eq. (5) in the main text, $Q_b^x \approx -h^x/4D\alpha^2$, which after substitution into previous expressions gives Eqs. (18-19) in the main text.